regional mantle response. For sites far from the ice sheets, the primary contribution is from the regional response to the change in water load, although there remains a component of global flow in response to the distant glacial unloading, and the resulting viscosity estimate will partly reflect mantle conditions beneath the ice sheets. Likewise, for sites near the rebound centers, the response will be largely determined by the mantle beneath the ice load, but there will remain a smaller component that is determined by mantle conditions further away. Thus, although the regional results should indicate whether lateral variation is likely to be important, they will not lead to definitive values.

80. M. Nakada, K. Lambeck, in *Glacial Isostasy, Sea-level and Mantle Rheology*, R. Sabadini, K. Lambeck, E. Boschi, Eds. (Kluwer, Dordrecht, Netherlands, 1991), pp. 79–94.
81. W. R. Peltier, *Science* **265** 195 (1994).
82. K. Lambeck, *J. Geol. Soc. London* **152**, 437 (1995).
83. _____, *Antiquity* **70**, 588 (1996).
84. _____, *Earth Planet. Sci. Lett.* **142**, 43 (1996).
85. T. W. Jacobson, *Sci. Am.* **234**, 343 (1976).
86. T. H. van Andel, in *Landscapes and People of the Franchthi Region*, T. W. Jacobson, Ed. (Indiana Univ. Press, Bloomington, IN, 1987), pp. 3–64.
87. G. Roux, *Ancient Iraq* (Penguin, London, 1992).
88. G. Roux, in *Initiation in l'Orient Ancien*, J. Bottéro, Ed. (Editions du Seuil, Paris, 1992), pp. 37–56.
89. R. Jones, *Annu. Rev. Anthropol.* **24**, 423 (1995).
90. R. Cosgrove, J. Allen, B. Marshall, *Antiquity* **64**, 59 (1990).
91. J. F. O'Connell, J. Allen, *Evol. Anthropol.* **6**, 132 (1998).
92. A. Thorne *et al.*, *J. Hum. Evol.* **36**, 591 (1999).
93. R. Grün *et al.*, *J. Hum. Evol.* **38**, 733 (2000).
94. J. Gibb, *R. Soc. N. Z. Bull.* **24**, 377 (1986).
95. P. L. Woodworth *et al.*, *Geophys. J. Int.* **136**, 651 (1999).
96. M. Ekman, *Global Planet. Change* **21**, 215 (1999).

REVIEW

Trends, Rhythms, and Aberrations in Global Climate 65 Ma to Present

James Zachos,[1]* Mark Pagani,[1] Lisa Sloan,[1] Ellen Thomas,[2,3] Katharina Billups[4]

Since 65 million years ago (Ma), Earth's climate has undergone a significant and complex evolution, the finer details of which are now coming to light through investigations of deep-sea sediment cores. This evolution includes gradual trends of warming and cooling driven by tectonic processes on time scales of 10^5 to 10^7 years, rhythmic or periodic cycles driven by orbital processes with 10^4- to 10^6-year cyclicity, and rare rapid aberrant shifts and extreme climate transients with durations of 10^3 to 10^5 years. Here, recent progress in defining the evolution of global climate over the Cenozoic Era is reviewed. We focus primarily on the periodic and anomalous components of variability over the early portion of this era, as constrained by the latest generation of deep-sea isotope records. We also consider how this improved perspective has led to the recognition of previously unforeseen mechanisms for altering climate.

Through study of sedimentary archives, it has become increasingly apparent that during much of the last 65 million years and beyond, Earth's climate system has experienced continuous change, drifting from extremes of expansive warmth with ice-free poles, to extremes of cold with massive continental ice-sheets and polar ice caps. Such change is not unexpected, because the primary forces that drive long-term climate, Earth's orbital geometry and plate tectonics, are also in perpetual motion. Much of the higher frequency change in climate (10^4 to 10^5 years) is generated by periodic and quasi-periodic oscillations in Earth's orbital parameters of eccentricity, obliquity, and precession that affect the distribution and amount of incident solar energy (Fig. 1) (*1*). Whereas eccentricity affects climate by modulating the amplitude of precession and thus influencing the total annual/seasonal solar energy budget, obliquity changes the latitudinal distribution of insolation. Because the orbital parameters vary with distinct tempos that remain stable for tens of millions of years (*2*), they provide a steady and, hence, predictable pacing of climate.

The orbitally related rhythms, in turn, oscillate about a climatic mean that is constantly drifting in response to gradual changes in Earth's major boundary conditions. These include continental geography and topography, oceanic gateway locations and bathymetry, and the concentrations of atmospheric greenhouse gases (*3*). These boundary conditions are controlled largely by plate tectonics, and thus tend to change gradually, and for the most part, unidirectionally, on million-year (My) time scales. Some of the more consequential changes in boundary conditions over the last 65 My include: North Atlantic rift volcanism, opening and widening of the two Antarctic gateways, Tasmanian and Drake Passages (*4*); collision of India with Asia and subsequent uplift of the Himalayas and Tibetan Plateau (*5*); uplift of Panama and closure of the Central American Seaway (*6*) (Figs. 1 and 2); and a sharp decline in pCO_2 (*7*). Each of these tectonically driven events triggered a major shift in the dynamics of the global climate system (*8–15*). Moreover, in altering the primary boundary conditions and/or mean climate state, some or all of these events have altered system sensitivity to orbital forcing (*16*), thereby increasing the potential complexity and diversity of the climate spectrum. This would include the potential for unusually rapid or extreme changes in climate (*17, 18*).

Although Earth's climatic history has been reconstructed with an array of proxies applied to both marine and terrestrial sediment archives, much of the progress in resolving the rates and scales of Cenozoic climate change can be attributed to the development of high-resolution deep-sea oxygen ($\delta^{18}O$) and carbon ($\delta^{13}C$) isotope records (*19*). Since the early 1970s, $\delta^{18}O$ data have served as the principal means of reconstructing global and regional climate change on a variety of geologic time-scales, from millennial to tectonic. These records are multidimensional in that they provide both climatic and stratigraphic information, and can be quickly generated with automated mass spectrometers. The first marine isotope records were relatively coarse, but still provided valuable insight into the general structure of the Pleistocene glacial and interglacial cycles (*20*). These were followed by records delineating the long-term patterns of Cenozoic climate change (*21–23*) and, eventually, the first global compilation of records for the Cenozoic (resolution of 10^5 to 10^6 years) (*24*).

The last decade has witnessed a rapid growth in the inventory of high-resolution isotope records across the Cenozoic, aided by the greater availability of high-quality sediment cores recovered by the Deep Sea Drilling Project (DSDP) and Ocean Drilling Program (ODP). The improved perspective provided by these records has led to some of the most exciting scientific developments of the

[1]Earth Sciences Department, University of California, Santa Cruz, CA 95064, USA. [2]Department of Earth and Environmental Sciences, Wesleyan University, Middletown, CT 06459, USA. [3]Center for the Study of Global Change, Yale University, New Haven, CT 06520–8105, USA. [4]College of Marine Studies, University of Delaware, Lewes, DE 19958, USA.

*To whom correspondence should be addressed. E-mail: jzachos@es.ucsc.edu

last decade, including the discovery of geologically abrupt shifts in climate, as well as "transient" events, brief but extreme excursions often associated with profound impacts on global environments and the biosphere (*25–28*). Moreover, these high-fidelity deep-sea records have facilitated efforts to extend the "astronomically calibrated" geological time scale back into the early Cenozoic (*29, 30*), an achievement previously considered difficult, if not impossible. Carbon isotope data have proved to be equally invaluable for stratigraphic correlation, and for providing insight into the operation of the global carbon cycle (*31*). In essence, by detailing both the rate and magnitude of past environmental perturbations, the latest generation of Cenozoic deep-sea isotope records has opened windows into a climatically dynamic period in Earth history. This, in turn, has proven invaluable for developing and testing new theories on mechanisms of past climate change (*32–34*), and for providing the framework to assess the influence of climate on the environment (*35*).

The Deep-Sea Stable Isotope Record

As a framework for this review, oxygen and carbon isotope data for bottom-dwelling, deep-sea foraminifera from over 40 DSDP and ODP sites representing various intervals of the Cenozoic were culled from the literature and compiled into a single global deep-sea isotope record (Fig. 2) [Web table 1 (*36*)]. The numerical ages are relative to the standard geomagnetic polarity time scale (GPTS) for the Cenozoic [Web note 1 (*36*)] (*37*). To facilitate visualization and minimize biases related to inconsistencies in sampling density in space and time, the raw data were smoothed and curve-fitted with a locally weighted mean. The smoothing results in a loss of detail that is undetectable in the long-time scale perspective. The oxygen isotope data provide constraints on the evolution of deep-sea temperature and continental ice volume [Web note 2 (*36*)]. Because deep ocean waters are derived primarily from cooling and sinking of water in polar regions, the deep-sea temperature data also double as a time-averaged record of high-latitude sea-surface temperatures (SST). The deep-sea carbon isotope data, on the other hand, provide insight into the nature of global carbon cycle perturbations [Web note 2 (*36*)] (*38*), and on first-order changes in deep-sea circulation patterns [Web note 3 (*36*)] (*39*) that might trigger or arise from the climatic changes.

Cenozoic Climate: From Greenhouse to Icehouse

Our benthic compilation shows a total $\delta^{18}O$ range of 5.4‰ over the course of the Cenozoic (Fig. 2). Roughly ~3.1‰ of this reflects deep-sea cooling, the remainder growth of ice-sheets, first on Antarctica (~1.2‰), and then in the Northern Hemisphere (~1.1‰). We consider the climate evolution depicted by this record under three categories: (i) long-term (~10^6 to 107 years), (ii) short-term or orbital-scale (~10^4 to 10^5 years), and (iii) aberrations or event-scale (~10^3 to 10^4 years).

Long-term trends. The $\delta^{18}O$ record exhibits a number of steps and peaks that reflect on episodes of global warming and cooling, and ice-sheet growth and decay (Fig. 2). The most pronounced warming trend, as expressed by a 1.5‰ decrease in $\delta^{18}O$, occurred early in the Cenozoic, from the mid-Paleocene (59 Ma) to early Eocene (52 Ma), and peaked with the early Eocene Climatic Optimum (EECO; 52 to 50 Ma). The EECO was followed by a

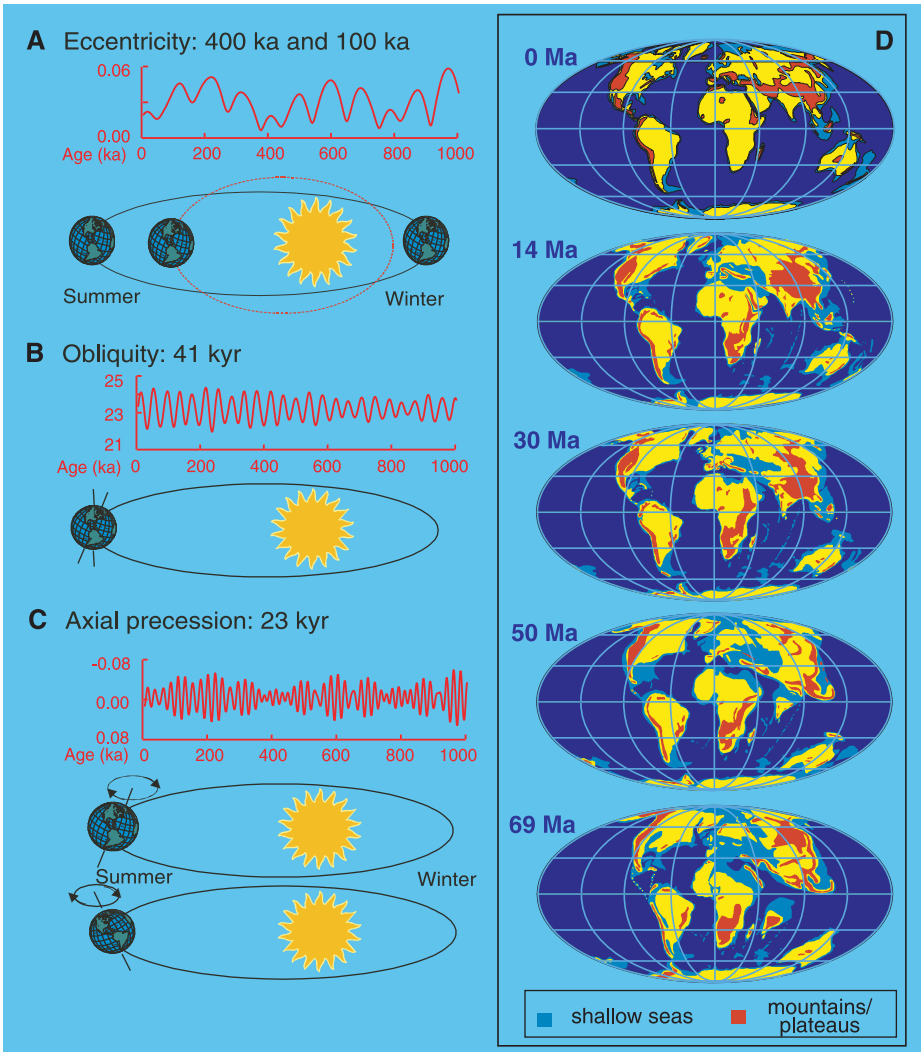

Fig. 1. Primary orbital components are displayed on the left, and Cenozoic paleogeography on the right. The gravitational forces exerted by other celestial bodies affect Earth's orbit. As a result, the amount and, more importantly, the distribution of incoming solar radiation oscillate with time (*123*). There are three orbital perturbations with five periods: eccentricity (at 400 and 100 ky), obliquity (41 ky), and precession (23 and 19 ky). (**A**) Eccentricity refers to the shape of Earth's orbit around the sun, varying from near circular to elliptical. This effect on insolation is very small, however, and by itself should not account for changes in Earth's climate during the past. (**B**) Obliquity refers to the tilt of Earth's axis relative to the plane of the ecliptic varying between 22.1° and 24.5°. A high angle of tilt increases the seasonal contrast, most effectively at high latitudes (e.g., winters in both hemispheres will be colder and summers hotter as obliquity increases). (**C**) Precession refers to the wobble of the axis of rotation describing a circle in space with a period of 26 ky. Modulated by orbital eccentricity, precession determines where on the orbit around the sun (e.g., with relation to aphelion or perihelion) seasons occur, thereby increasing the seasonal contrast in one hemisphere and decreasing it in the other. The effect is largest at the equator and decreases with increasing latitude. The periods of the precessional signal modulated by eccentricity are 23 and 19 ky, the periods observed in geological records. (**D**) Continental geography reconstructed for five intervals of the last 70 My (designed using the commercial Paleogeographic Information System).

17-My-long trend toward cooler conditions as expressed by a 3.0‰ rise in $\delta^{18}O$ with much of the change occurring over the early-middle (50 to 48 Ma) and late Eocene (40 to 36 Ma), and the early Oligocene (35 to 34 Ma). Of this total, the entire increase in $\delta^{18}O$ prior to the late Eocene (~1.8‰) can be attributed to a 7.0°C decline in deep-sea temperature (from ~12° to ~4.5°C). All subsequent $\delta^{18}O$ change reflects a combined effect of ice-volume and temperature (*40*), particularly for the rapid >1.0‰ step in $\delta^{18}O$ at 34 Ma. On the basis of limits imposed by bottom-water and tropical temperatures, it has been estimated that roughly half this signal (~0.6‰) must reflect increased ice volume (*24, 41*), though independent constraints on temperature derived from benthic foraminiferal Mg/Ca ratios argue for a slightly greater ice-volume component (~0.8 to 1.0‰) (*42*). This long-term pattern of deep-sea warming and cooling is consistent with reconstructions of early Cenozoic subpolar climates based on both marine and terrestrial geochemical and fossil evidence (*43–47*).

Following the cooling and rapid expansion of Antarctic continental ice-sheets in the earliest Oligocene, deep-sea $\delta^{18}O$ values remained relatively high (>2.5‰), indicating a permanent ice sheet(s), likely temperate in character (*48*), with a mass as great as 50% of that of the present-day ice sheet and bottom temperatures of ~4°C (*18*). These ice sheets persisted until the latter part of the Oligocene (26 to 27 Ma), when a warming trend reduced the extent of Antarctic ice. From this point until the middle Miocene (~15 Ma), global ice volume remained low and bottom water temperatures trended slightly higher (*49, 50*), with the exception of several brief periods of glaciation (e.g., Mi-events) (*39*). This warm phase peaked in the late middle Miocene climatic optimum (17 to 15 Ma), and was followed by a gradual cooling and reestablishment of a major ice-sheet on Antarctica

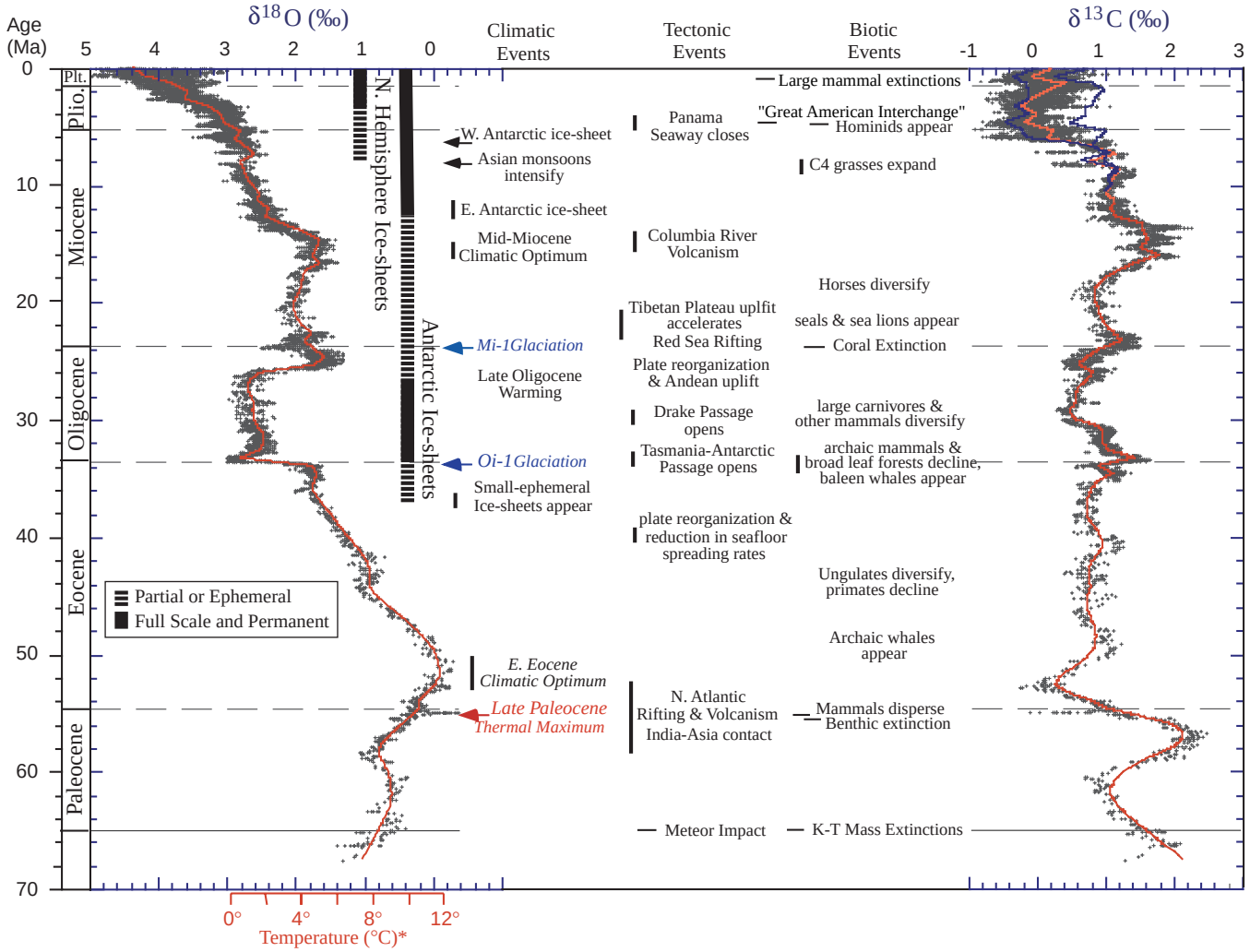

Fig. 2. Global deep-sea oxygen and carbon isotope records based on data compiled from more than 40 DSDP and ODP sites (*36*). The sedimentary sections from which these data were generated are classified as pelagic (e.g., from depths >1000 m) with lithologies that are predominantly fine-grained, carbonate-rich (>50%) oozes or chalks. Most of the data are derived from analyses of two common and long-lived benthic taxa, *Cibicidoides* and *Nuttallides*. To correct for genus-specific isotope vital effects, the $\delta^{18}O$ values were adjusted by +0.64 and +0.4‰ (*124*), respectively. The absolute ages are relative to the standard GPTS (*36, 37*). The raw data were smoothed using a five-point running mean, and curve-fitted with a locally weighted mean. With the carbon isotope record, separate curve fits were derived for the Atlantic (blue) and Pacific above the middle Miocene to illustrate the increase in basin-to-basin fractionation that exceeds ~1.0‰ in some intervals. Prior to 15 Ma, interbasin gradients are insignificant or nonexistent (*39*). The $\delta^{18}O$ temperature scale was computed for an ice-free ocean [~1.2‰ Standard Mean Ocean Water (SMOW)], and thus only applies to the time preceding the onset of large-scale glaciation on Antarctica (~35 Ma) (*43*). From the early Oligocene to present, much of the variability (~70%) in the $\delta^{18}O$ record reflects changes in Antarctica and Northern Hemisphere ice volume (*40*). The vertical bars provide a rough qualitative representation of ice volume in each hemisphere relative to the LGM, with the dashed bar representing periods of minimal ice coverage (≲50%), and the full bar representing close to maximum ice coverage (>50% of present). Some key tectonic and biotic events are listed as well (*4, 5, 35*).

by 10 Ma (*51, 52*). Mean $\delta^{18}O$ values then continued to rise gently through the late Miocene until the early Pliocene (6 Ma), indicating additional cooling and small-scale ice-sheet expansion on west-Antarctica (*53*) and in the Arctic (*54*). The early Pliocene is marked by a subtle warming trend (*55*) until ~3.2 Ma, when $\delta^{18}O$ again increased reflecting the onset of Northern Hemisphere Glaciation (NHG) (*56, 57*).

Rhythms. Given this framework for long-term trends, how has the tempo and amplitude of orbital scale climate variability evolved through the Cenozoic, particularly during the transitions between different glacial states (unipolar to bipolar)? To address this, we turn to high-resolution time-series spanning four intervals: 0.0 to 4.0, 12.5 to 16.5, 20.5 to 24.5, and 31.0 to 35.0 Ma, each representing an interval of major continental ice-sheet growth or decay. The time-series are from DSDP and ODP Sites 659 [0 to 4 Ma (*58*)], 588 [12.5 to 16.5 Ma (*59*)], 929 [20.5 to 24.5 (*60*)], and 522 [31 to 35 Ma (*61, 62*)] (Fig. 3). Two of the records, Sites 659 and 929, have orbitally tuned age models. The mean sampling density varies from roughly 2 ky for the 0- to 4-Ma time slice to 9 ky for the 31- to 35-Ma time slice, thereby limiting resolution of the high-frequency orbital-scale periodicities in the oldest intervals. Nevertheless, resolution is high enough to avoid signal aliasing of lower frequency periods.

These and other benthic $\delta^{18}O$ time-series demonstrate that climate varies in a quasi-periodic fashion during all intervals characterized by glaciation, regardless of the location and extent of ice-sheets. In terms of frequency, much of the power in the climate spectrum since the early Oligocene appears to be concentrated in the obliquity band (~40 ky) (Fig. 4). Additional power resides in the eccentricity bands, although the signal strength is more variable. For example, $\delta^{18}O$ variance in the 100-ky frequency band is exceptionally pronounced over the last 800 to 900 ky following a mid-Pleistocene shift (*63*), but weaker through the early Pleistocene and Pliocene when the signal was dominated by variance in the 41-ky band (*64, 65*). Similar secular shifts in the power of the 100-ky cycle occurred in the late Oligocene and early Miocene. Power in the 400-ky band is exceptionally pronounced in the early Miocene, whereas it is relatively weak in the Pleistocene (*66, 67*), and early Oligocene (*61, 68*).

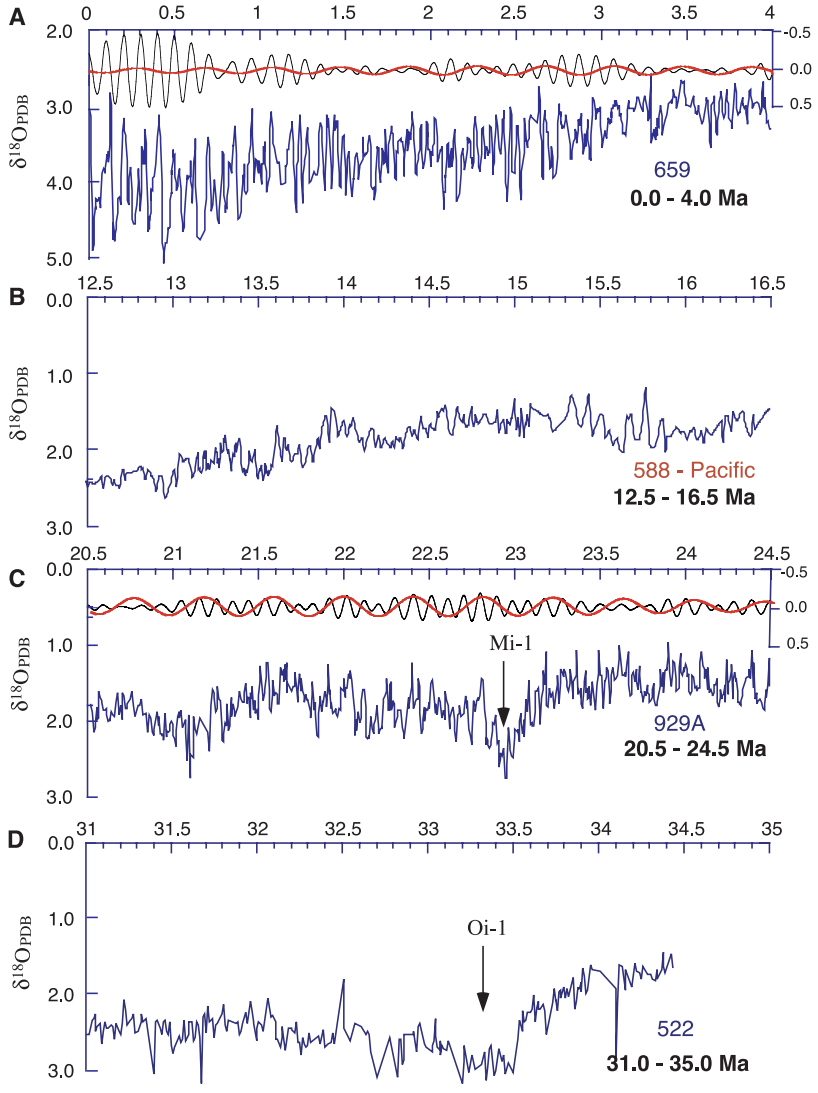

Fig. 3. (**A** through **D**) High-resolution 4-My-long $\delta^{18}O$ time series representing four intervals of the Cenozoic. The data are from Site 659, eastern equatorial Atlantic (*58*); Site 588, southwest Pacific (*59*); Site 929, western equatorial Atlantic (*60*); Site 522, south Atlantic (*61*); and Site 689, Southern Ocean (*68*). Sampling intervals range from 3 to 10 ky. Note that the $\delta^{18}O$ axes on all plots are set to the same scale (3.0‰), though at different ranges to accommodate the change in mean ocean temperature/ice volume with time. The Plio-Pleistocene ages for Site 659 are constrained by oxygen isotope records directly or indirectly calibrated to Northern Hemisphere summer insolation at 65°N, based on the astronomical solutions of Berger and Loutre (*123*). The Site 929 age model is also calibrated to an orbital curve derived from the formulations of Laskar (*2*) with corrections for tidal dissipation (*29*). The upper curves in (A) and (C) represent Gaussian band-pass filters designed to isolate variance associated with the 400- and 100-ky eccentricity cycles. The 400-ky filter has a central frequency = 0.0025 and a bandwidth = 0.0002; the 100-ky central frequency = 0.01 and bandwidth = 0.002. Filters were not constructed for the two records, at sites 588 and 522, which have not been orbitally tuned.

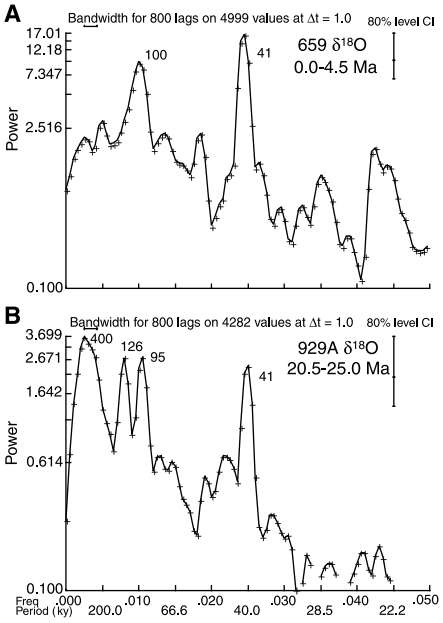

Fig. 4. Spectral density as a function of frequency for (**A**) the Plio-Pleistocene (0 to 4 Ma) and (**B**) Oligocene-Miocene (20.5 to 24.5), as based on the benthic $\delta^{18}O$ time series of Sites 659 and 929. The analyses were performed using the Blackman-Tuckey method (Arand Software). Both records were detrended and resampled at 1-ky steps. Both records have been tuned to the orbital spectrum Atlantic [Web note 1 (*36*)] (*58, 60*).

The variations in the amplitude of the Cenozoic deep sea $\delta^{18}O$ signal largely reflect on changes in continental ice-volume and temperature. For example, the largest oscillations are recorded over the last 800 ky during the period of maximum NHG. The most recent independent constraints on the isotopic composition of seawater during the last major ice advance (20 ka) suggest that <1.0‰ of the total range of ~2.4‰ for this period may reflect changes in ice volume, the remainder temperature (*69, 70*). Conversely, the lowest amplitude oscillations (~0.2 to 0.3‰) were in the late Eocene prior to the appearance of permanent Antarctic ice-sheets. Slightly higher amplitude oscillations (~0.5‰) occurred in the early Oligocene, late Miocene (*71*), and early Pliocene (*72*), when Antarctica was close to fully glaciated. Conversely, larger amplitude (0.5 to 1.0‰) oscillations are recorded in the latest Oligocene and early Miocene, the period when Antarctica was minimally or only partially glaciated.

Aberrations. Perhaps the most interesting and unexpected discoveries of the last decade are the aberrations. These are loosely defined as brief (~10^3 to 10^5 y) anomalies that stand out well above "normal" background variability in terms of rate and/or amplitude, and are usually accompanied by a major perturbation in the global carbon cycle as inferred from carbon isotope data. The three largest occurred at ~55, 34, and 23 Ma, all near or at epoch boundaries. This last distinction is significant in that it implies that each of these climate events may have also had widespread and long-lasting impacts on the biosphere.

The most prominent of the climatic aberrations is the Late Paleocene Thermal Maximum (LPTM), which occurred at 55 Ma near the Paleocene/Eocene (P/E) boundary. This event is characterized by a 5° to 6°C rise in deep-sea temperature (>1.0‰ negative isotope excursion) in less than 10 ky (Fig. 5) (*25, 26, 73*). Sea surface temperatures as constrained by planktonic isotope records also increased, by as much as 8°C at high latitudes and lesser amounts toward the equator (*47, 74, 75*). Recovery was gradual, taking ~200 ky from the onset of the event (*30*). An associated notable change in climate was globally higher humidity and precipitation, as evidenced by changes in the character and patterns of continental weathering (*76, 77*). The event is also characterized by a ~3.0‰ negative carbon isotope excursion of the marine, atmospheric, and terrestrial carbon reservoirs (Fig. 5) (*25, 78–80*); widespread dissolution of seafloor carbonate (*75, 81*); mass extinction of benthic foraminifera (*82*); widespread proliferation of exotic planktic foraminifera taxa (*74, 83*) and the dinoflagellate *Apectodinium* (*84*); and the dispersal and subsequent radiation of Northern Hemisphere land plants and mammals (*78, 85–88*). The recovery interval is marked by a possible rise in marine and terrestrial productivity and organic carbon deposition (*89, 90*).

In contrast, the next two climatic aberrations are characterized by positive oxygen isotope excursions that reflect brief extremes in Antarctic ice-volume and temperature (*27, 61*). The first of these lies just above the Eocene/Oligocene boundary (34.0 Ma) (Fig. 3). It is a 400-ky-long glacial that initiated with the sudden appearance of large continental ice sheets on Antarctica. This transition, referred to as Oi-1 (*50*), appears to involve reorganization of the climate/ocean system as evidenced by global wide shifts in the distribution of marine biogenic sediments and an overall increase in ocean fertility (*62, 91, 92*), and by a major drop in the calcium carbonate compensation depth (*93, 94*). The second aberration coincided with the Oligocene/Miocene boundary (~23 Ma) (*95*) and consists of a brief but deep (~200 ky) glacial maximum (Fig. 3) (*60*). This event, referred to as Mi-1 (*50*), was followed by a series of intermittent but smaller glaciations. Both Oi-1 and Mi-1 were accompanied by accelerated rates of turnover and speciation in certain groups of biota, although on a smaller scale than at the LPTM (*96*). Of particular significance are the rise of modern whales (i.e., baleen) and shift in continental floral communities at the E/O boundary (*97, 98*), and the extinction of Caribbean corals at the O/M boundary (*99*). Furthermore, both transients are characterized by small but sharp positive carbon isotope excursions (~0.8‰) suggestive of perturbations to the global carbon cycle (Fig. 2). Although records indicate a number of lesser events in the Oligocene and Miocene, none appear to approach Oi-1 and Mi-1 events in terms of magnitude.

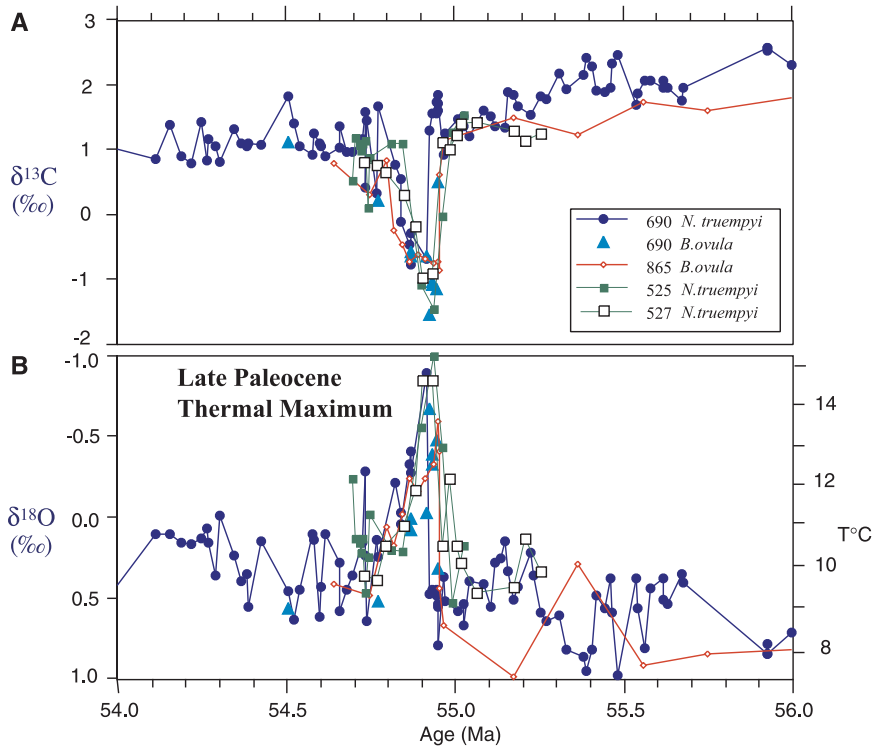

Fig. 5. The LPTM as recorded in benthic $\delta^{13}C$ and $\delta^{18}O$ records (**A** and **B**, respectively) from Sites 527 and 690 in the south Atlantic (*73*), and Site 865 in the western Pacific (*26*). The time scale is based on the cycle stratigraphy of Site 690 (*30*) with the base of the excursion placed at 54.95 Ma. The other records have been correlated to Site 690 using the carbon isotope stratigraphy. Apparent leads and lags are artifacts of differences in sample spacing. The oxygen isotope values have been adjusted for species-specific vital effects (*118*), and the temperature scale on the right is for an ice-free ocean. The negative carbon isotope excursion is thought to represent the influx of up to 2600 Gt of methane from dissociation of seafloor clathrate (*111*).

Implications for Climate Forcing Mechanisms

Has the greater temporal resolution of Cenozoic climate afforded by the latest isotope reconstructions altered our understanding of the nature of long- and short-term climate change? The answer to this is both yes and no. Perhaps the most important developments concern the glacial history of Antarctica, and the scale and timing of climatic aberrations. In the case of the former, it is evident that ice sheets have been present on Antarctica for the last 40 My, and over much of that time have been extremely dynamic, implying a high degree of instability and/or sensitivity to forcing. As for the aberrations, their mere existence points toward the potential for highly nonlinear responses in climate to forcing, or

the possibility of unexpected anomalies in forcing.

Gateways or pCO_2? With the previous less-detailed perspective of Cenozoic climate—that is, warm and ice-free in the beginning to cold and glaciated at present—there was tendency to attribute the unidirectional trend, Cenozoic cooling, to a single factor such as the increased thermal isolation of Antarctica due to the increased widening of the oceanic passages. However, as the complex nature of the long-term trend comes into focus, it is becoming clear that more than one factor was responsible. A case in point is the transition into and out of the long-term Oligocene glaciation. Thermal isolation of Antarctica by widening oceanic passages may explain the initial appearance of Antarctic ice-sheets, but fails to explain the subsequent termination. New reconstructions of Cenozoic pCO_2 (Fig. 6) (*7, 100*) have added another dimension to this argument, indicating that this termination occurred at a time when greenhouse gas levels were declining or already relatively low. This reinforces the notion that moisture supply was the critical element in maintaining large polar ice-sheets, at least during the middle Cenozoic (*101, 102*). Although globally averaged precipitation should covary with pCO_2, on regional scales other parameters such as circulation patterns need to be considered as well. Future efforts to model the onset of Oligocene glaciation should investigate the role of the hydrological cycle in maintaining large ice-sheets on an otherwise warmer than present Antarctic continent. Similarly, with low pCO_2 over the last 25 My, tectonic events such as mountain building or oceanic gateway reconfigurations, which can alter ocean/atmosphere circulation and heat and vapor transport, may have had a dominant role in triggering large-scale shifts in climate (*10, 11, 103*). Conversely, at these low levels, subtle changes in pCO_2, at least within the error of the proxy estimates, may be important in triggering ice-volume changes, again not just through influences on radiative forcing, but also on atmospheric circulation patterns and humidity. Clearly, in the case of long-term trends, with so many variables, some still not well constrained (i.e., pCO_2, approximate timing of tectonic events), the task of relating response to forcing is still far from complete.

Orbital pacing. Efforts to relate periodic climate variability to forcing through the Cenozoic have proven to been far more successful. For example, it is now evident that the primary beat of the glaciated Cenozoic is in the obliquity band, regardless of the state of other boundary conditions or the location of ice sheets (e.g., Fig. 4). This is true for the lower frequency 1.25-My period of obliquity as well (*104*). This observation confirms the highly sensitive nature of ice-sheets to obliquity-generated changes in high-latitude insolation, particularly when the polar regions (i.e., Antarctica) are only partially ice-covered, as in the Miocene. Although the benthic isotope records currently available for the ice-free Cenozoic lack adequate resolution to fully characterize obliquity variance, other proxy records (i.e., physical properties) suggest that the global climatic response was dominated by variance in the precession-related bands (*30, 105*). This supports the notion that the overall influence of obliquity on global climate during ice-free periods, without an ice-sheet amplifier, is weaker or less apparent.

A more definitive finding, however, is the verification of a strong pre-Pleistocene climate response to eccentricity oscillations, as exemplified by the concentration of power at the 100- and 400-ky periods (*27, 67*). Analyses of the climate signal over those intervals where it is pronounced (i.e., the Miocene) reveal a high degree of coherency with eccentricity in terms of frequency and amplitude modulation. This finding supports the class of models that relate amplification of power in the eccentricity bands to the filtering effects of continental geography and differences in land-sea heating on precession, especially in the tropics (*16*). Here, power (temperature) can be shifted into the primary eccentricity bands via truncation of the cooler portion of precession-related insolation change. What remains unclear is how these effects are then exported to higher latitudes. Researchers have considered a variety of mechanisms for directly and indirectly amplifying the response to precession forcing (*106–109*). This includes processes such as ocean and atmospheric circulation that directly or indirectly influence heat-transport, precipitation, and/or the global carbon cycle and pCO_2. Of these, the carbon cycle is most appealing because of its long time constants, but is difficult to verify because of the large number of variables involved. Still, support for a carbon cycle amplifier is provided by Oligocene-Miocene carbon isotope records, which exhibit pervasive large-amplitude 100- and 400-ky oscillations that are highly coherent with the glacial cycles (*60*). Furthermore, reanalysis of ice-core data and other records indicate that the primary response to eccentricity in the late Pleistocene benthic $\delta^{18}O$ record is in temperature, not ice volume as originally believed, and that ice volume lagged eccentricity forcing, CO_2, and deep-sea temperature by the appropriate phase (*70*).

Thresholds, methane eruptions, and orbital anomalies. Characterizing the timing and scale of the three aberrations discussed here in the context of longer-term background paleoenvironmental variability has been critical to the development and testing of hypotheses on their origins. To begin with, each aberration was superimposed on a long-term gradual trend in the same direction. In terms of tempo, the step into the LPTM was much more abrupt ($\sim 10^3$ to 10^4 years) than that into the Oi-1 and Mi-1 events ($\sim 10^5$ years), and the recovery more gradual. This, and the fact that the direction of climatic change is opposite (e.g., a warming instead of cooling), hints at a different mechanism. For the LPTM, the abrupt negative ~3.0‰ global carbon isotope excursion (CIE) (Fig. 5) implicates a rise in greenhouse gas concentrations, most likely from the dissociation and subsequent oxidation of 2000 to 2600 Gt of isotopically light (~−60‰) methane from marine clathrates as proposed by Dickens *et al.* (*33, 110*). The carbon mass from this is consistent with a reduction in ocean pH as inferred from evidence for seafloor carbonate dissolution (*111, 112*). Although other sources of CO_2 have been considered (i.e., volcanic), the much greater masses required to generate the CIE would alter ocean chemistry to an extent unsupported by data. Why would such a large mass of methane hydrate suddenly dissociate at 55 Ma? Suggested triggering mechanisms range from the gradual

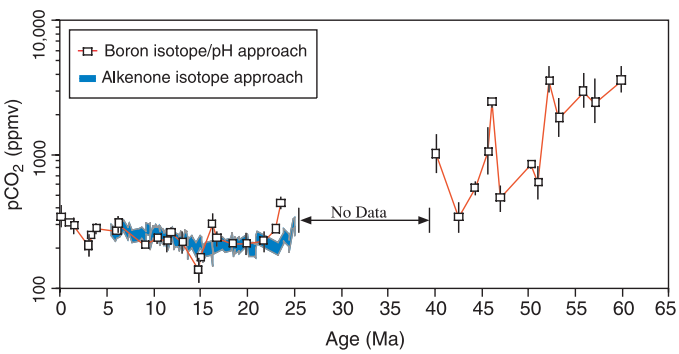

Fig. 6. Estimates of Cenozoic atmospheric pCO_2 based on two independent proxies as measured in subtropical deep-sea sediment cores from the Pacific. The first curve spanning most of the Cenozoic is estimated from surface ocean pH as derived from the boron isotope ratios of planktonic foraminifers (*7*). The second pCO_2 curve spanning the Miocene is based on the $\delta^{13}C$ values of phytoplankton organic compounds known as alkenones (*100*). Both approaches assume chemical equilibrium between the ocean and atmosphere. In the intervals of overlap, both proxies provide nearly identical estimates of paleo-pCO_2.

crossing of a thermal threshold via long-term deep-sea warming (*110*), to more abrupt deep-sea warming resulting from sudden changes in ocean circulation (*113, 114*), to massive regional slope failure (*115*).

In contrast to the LPTM, the much smaller magnitude and positive carbon isotope excursions for the Oi-1 and Mi-1 events indicate that greenhouse gas forcing was probably not the primary causal mechanism, but instead may have served as a positive or amplifying feedback. In this scenario, tectonic forcing is viewed at the primary triggering mechanism that drives the climate system across a physical threshold (i.e., temperature), which then initiates rapid growth of ice-sheets along with reorganization of ocean/atmosphere circulation (*17*). The physical changes, in turn, trigger large-scale biogeochemical feedbacks in the carbon cycle that initially amplify the climatic changes (*18*). Such feedbacks would be short-lived, because other coupled biogeochemical processes would eventually restore equilibrium to the system.

Orbital forcing may have had a hand in triggering these events as well, possibly as a means of providing the climate system with a final and relatively rapid push across a climatic threshold, or even as the principal driving force. For example, the Mi-1 event appears to be in phase with a long series of regular low-frequency oscillations (i.e., ~400 ky cycles) (*27*). Comparison of the Site 929 isotope records with the orbital curve (*2*), revealed that the low-frequency (400 ky) glacial maxima, including Mi-1, coincided with, and hence, were being paced by eccentricity minima (*60*). A normal cycle of low eccentricity, however, fails to explain the unusual amplitude of Mi-1. What is unusual is the congruence this low in eccentricity with a protracted node in obliquity (*34*). This rare orbital alignment involved four consecutive cycles of low-amplitude variance in obliquity (a node) coincident with the low eccentricity that resulted in an extended period (~200 ky) of cool summer orbits, and possibly, ice-sheet expansion on Antarctica.

In sum, it now appears that extreme aberrations in global climate can arise through a number of mechanisms. This would explain both the random distribution and frequency of such events over time. Some, such as rare anomalies in Earth's orbit, are predictable, at least to the extent that the orbital computations are correct. Others, like catastrophic methane release, are less so, although closer scrutiny of earlier time intervals when boundary conditions were similar to those preceding the LPTM might reveal the existence of similar aberrations (*116*). Correlation does not necessarily prove causation, but in the case of aberrations, the short time scales involved significantly reduces the number of potential variables, thereby rendering the task of identifying and testing mechanisms a more tractable proposition. Moreover, the abrupt transitions and transients offer a unique opportunity to study the dynamics of a rapidly changing climate system, as well as the response of the biosphere and biogeochemical cycles on global or regional scales to significant, sudden changes in greenhouse gas levels. To this end, future efforts should concentrate on establishing, in greater temporal detail, the global- and regional-scale changes associated with these short-lived events, particularly in climatically and/or environmentally sensitive regions, both marine and terrestrial (i.e., high latitudes, tropics, marginal seas, and continental interiors).

References and Notes

1. J. D. Hays, J. Imbrie, N. J. Shackleton, *Science* **194**, 1121 (1976).
2. J. Laskar, F. Joutel, F. Boudin, *Astron. Astrophys.* **270**, 522 (1993).
3. T. J. Crowley, K. G. Burke, Eds., *Tectonic Boundary Conditions for Climate Reconstructions*, vol. 39 (Oxford Univ. Press, New York, 1998).
4. L. A. Lawver, L. M. Gahagan, in (*3*), pp. 212–226.
5. P. Copeland, in (*15*), pp. 20–40.
6. G. H. Haug, R. Tiedemann, *Nature* **393**, 673 (1998).
7. P. N. Pearson, M. R. Palmer, *Nature* **406**, 695 (2000).
8. E. J. Barron, W. H. Peterson, *Palaeogeogr. Palaeoclimatol. Palaeoecol.* **83**, 1 (1991).
9. M. E. Raymo, W. F. Ruddiman, *Nature* **359**, 117 (1992).
10. J. E. Kutzbach, W. L. Prell, W. F. Ruddiman, *J. Geol.* **101**, 177 (1993).
11. U. Mikolajewicz, E. Maierreimer, T. J. Crowley, K. Y. Kim, *Paleoceanography* **8**, 409 (1993).
12. R. A. Berner, *Am. J. Sci.* **294**, 56 (1994).
13. L. C. Sloan, D. K. Rea, *Palaeogeogr. Palaeoclimatol. Palaeoecol.* **119**, 275 (1996).
14. U. Mikolajewicz, T. J. Crowley, *Paleoceanography* **12**, 429 (1997).
15. W. F. Ruddiman, Ed., *Tectonic Uplift and Climate Change* (Plenum, New York, 1997).
16. D. A. Short, J. G. Mengel, T. J. Crowley, W. T. Hyde, G. R. North, *Quat. Res.* **35**, 157 (1991).
17. T. J. Crowley, G. R. North, *Science* **240**, 996 (1988).
18. J. C. Zachos, K. C. Lohmann, J. C. G. Walker, S. W. Wise, *J. Geol.* **101**, 191 (1993).
19. All data are expressed in the delta notation δ (‰) = ($^{18}O/^{16}O_{samp}/^{18}O/^{16}O_{standard} - 1$)1000, and are reported relative to the VPDB (Vienna Pee Dee Belemnite) standard. The ratios of the stable isotopes of oxygen ($^{18}O/^{16}O$) in the calcite ($CaCO_3$) shells of marine organisms such as benthic foraminifera provide information on temperature and the isotopic composition of seawater (i.e., ice volume). In general, calcite $\delta^{18}O$ increases as temperature decreases (0.25‰/°C), or as the mass of continental ice increases (0.1‰/10 m sea-level change). The ratios of stable carbon isotopes ($^{13}C/^{12}C$) in benthic foraminifera, on the other hand, reflect on changes in the ratio of the dissolved inorganic carbon (DIC) of ambient seawater. Secular variations in the mean $\delta^{13}C_{DIC}$ of the ocean, in turn, reflect on changes in the rates of carbon supply and removal from organic and inorganic reservoirs [Web note 2 (*36*)] (*38*).
20. C. Emiliani, G. Edwards, *Nature* **171**, 887 (1953).
21. N. J. Shackleton, J. P. Kennett, in *Initial Reports of the Deep Sea Drilling Project* (U.S. Government Printing Office, Washington, DC, 1975), vol. 29, pp. 743–755.
22. S. M. Savin, R. G. Douglas, F. G. Stehli, *Geol. Soc. Am. Bull.* **86**, 1499 (1975).
23. R. K. Matthews, R. Z. Poore, *Bull. Am. Assoc. Petrol. Geol.* **65**, 954 (1981).
24. K. G. Miller, M. E. Katz, *Micropaleontology* **33**, 97 (1987).
25. J. P. Kennett, L. D. Stott, *Nature* **353**, 225 (1991).
26. T. J. Bralower *et al.*, *Paleoceanography* **10**, 841 (1995).
27. J. C. Zachos, B. P. Flower, H. Paul, *Nature* **388**, 567 (1997).
28. S. Bains, R. M. Corfield, R. D. Norris, *Science* **285**, 724 (1999).
29. N. J. Shackleton, S. J. Crowhurst, G. P. Weedon, J. Laskar, *Philos. Trans. R. Soc. London Ser. A* **357**, 1907 (1999).
30. U. Röhl, T. J. Bralower, R. D. Norris, G. Wefer, *Geology* **28**, 927 (2000).
31. L. R. Kump, M. A. Arthur, in (*15*), pp. 399–426.
32. L. C. Sloan, J. C. G. Walker, T. C. Moore, D. K. Rea, J. C. Zachos, *Nature* **357**, 320 (1992).
33. G. R. Dickens, J. R. O'Neil, D. K. Rea, R. M. Owen, *Paleoceanography* **10**, 965 (1995).
34. J. C. Zachos, N. J. Shackleton, J. S. Revenaugh, H. Pälike, B. P. Flower, *Science* **292**, 274 (2001).
35. J. Alroy, P. L. Koch, J. C. Zachos, in *Deep Time: Paleobiology's Perspective*, D. H. Erwin, S. L. Wing, Eds. (The Paleontological Society, Lawrence, KS, 2000), vol. 26, pp. 259–288.
36. Supplementary material is available at www.sciencemag.org/cgi/content/full/292/686/5517/DC1.
37. W. A. Berggren, D. V. Kent, C. C. I. Swisher, M.-P. Aubry, in *Geochronology Time Scales and Global Stratigraphic Correlation*, D. V. Kent, M.-P. Aubry, J. Hardenbol, Eds. (Society for Sedimentary Geology, Tulsa, OK, 1995), vol. 54, pp. 129–212.
38. N. J. Shackleton, *Geol. Soc. Spec. Publ.* **26**, 423 (1987).
39. J. D. Wright, K. G. Miller, in *The Antarctic Paleoenvironment: A Perspective on Global Change*, J. P. Kennet, D. A. Warnke, Eds. (American Geophysical Union, Washington, DC, 1993), pp. 1–25.
40. The presumption of a negligible contribution from ice sheets prior to the earliest Oligocene, and large ice-sheets thereafter, is supported by several lines of evidence, including the distribution of glaciomarine sediment or ice-rafted debris near or on Antarctica, and by changes in the distribution and abundances of clay minerals associated with physical weathering in proximal margin and deep-sea sediments (*47, 48, 117–122*).
41. J. C. Zachos, L. D. Stott, K. C. Lohmann, *Paleoceanography* **9**, 353 (1994).
42. C. H. Lear, H. Elderfield, P. A. Wilson, *Science* **287**, 269 (2000).
43. J. E. Francis, *Arctic* **41**, 314 (1988).
44. L. D. Stott, J. P. Kennet, *Proc. Ocean Drill. Program Sci. Results* **113**, 849 (1990).
45. E. Barrera, B. T. Huber, *Proc. Ocean Drill. Program Kerguelen Plateau Prydz Basin* **119**, 736 (1991).
46. P. W. Ditchfield, J. D. Marshall, D. Pirrie, *Palaeogeogr. Palaeoclimatol. Palaeoecol.* **107**, 79 (1994).
47. R. V. Dingle, S. A. Marenssi, M. Lavelle, *J. S. Am. Earth Sci.* **11**, 571 (1998).
48. M. J. Hambrey, W. U. Ehrmann, B. Larsen, *Proc. Ocean Drill. Program Sci. Results* **119**, 77 (1991).
49. J. D. Wright, K. G. Miller, R. G. Fairbanks, *Paleoceanography* **7**, 357 (1992).
50. K. G. Miller, J. D. Wright, R. G. Fairbanks, *J. Geophys. Res.* **96**, 6829 (1991).
51. E. Vincent, J. S. Killingley, W. H. Berger, *Geol. Soc. Am. Mem.* **163**, 103 (1985).
52. B. P. Flower, *Paleoceanography* **10**, 1095 (1995).
53. J. P. Kennett, P. F. Barker, *Proc. Ocean Drill. Program Sci. Results* **113**, 937 (1990).
54. J. Thiede, T. O. Vorren, *Mar. Geol.* **119**, 179 (1994).
55. R. Z. Poore, L. C. Sloan, *Mar. Micropaleontol.* **27**, 1 (1996).
56. N. J. Shackleton, J. Imbrie, N. G. Pisias, *Philos. Trans. R. Soc. London Ser. B* **318**, 679 (1988).
57. M. A. Maslin, X. S. Li, M. F. Loutre, A. Berger, *Quat. Sci. Rev.* **17**, 411 (1998).
58. R. Tiedemann, M. Sarnthein, N. J. Shackleton, *Paleoceanography* **9**, 619 (1994).
59. B. P. Flower, J. P. Kennett, *Palaeogeogr. Palaeoclimatol. Palaeoecol.* **108**, 537 (1994).
60. H. A. Paul, J. C. Zachos, B. P. Flower, A. Tripati, *Paleoceanography* **15**, 471 (2000).
61. J. C. Zachos, T. M. Quinn, K. A. Salamy, *Paleoceanography* **11**, 251 (1996).

62. K. A. Salamy, J. C. Zachos, *Palaeogeogr. Palaeoclimatol. Palaeoecol.* **145**, 61 (1999).
63. M. Mudelsee, K. Stattegger, *Geol. Rundsch.* **86**, 499 (1997).
64. W. F. Ruddiman, M. Raymo, A. McIntyre, *Earth Planet. Sci. Lett.* **80**, 117 (1986).
65. M. Raymo, W. F. Ruddiman, N. J. Shackleton, D. Oppo, *Earth Planet. Sci. Lett.* **97**, 353 (1992).
66. A. C. Mix *et al.*, *Proc. Ocean Drill. Program Sci. Results* **138**, 371 (1995).
67. S. C. Clemens, R. Tiedemann, *Nature* **385**, 801 (1997).
68. L. Diester-Haass, R. Zahn, *Geology* **24**, 163 (1996).
69. D. P. Schrag, G. Hampt, D. W. Murray, *Science* **272**, 1930 (1996).
70. N. J. Shackleton, *Science* **289**, 1897 (2000).
71. _____, M. Hall, *Proc. Ocean Drill. Program Sci. Results* **154**, 367 (1997).
72. K. Billups, A. C. Ravelo, J. C. Zachos, *Paleoceanography* **13**, 459 (1998).
73. E. Thomas, N. J. Shackleton, in *Correlation of the Early Paleogene in Northwest Europe*, R. O. Knox, R. M. Corfield, R. E. Dunay, Eds. (Geologic Society, London, 1996), vol. 247, pp. 481–496.
74. D. C. Kelly, T. J. Bralower, J. C. Zachos, I. P. Silva, E. Thomas, *Geology* **24**, 423 (1996).
75. D. J. Thomas, T. J. Bralower, J. C. Zachos, *Paleoceanography* **14**, 561 (1999).
76. C. Robert, J. P. Kennett, *Mar. Geol.* **103**, 99 (1992).
77. T. G. Gibson, L. M. Bybell, D. B. Mason, *Sediment. Geol.* **134**, 65 (2000).
78. P. L. Koch, J. C. Zachos, P. D. Gingerich, *Nature* **358**, 319 (1992).
79. R. M. Corfield, *Earth Sci. Rev.* **37**, 225 (1994).
80. D. Beerling, D. W. Jolley, *J. Geol. Soc. London* **155**, 591 (1998).
81. B. Schmitz *et al.*, *Palaeogeogr. Palaeoclimatol. Palaeoecol.* **133**, 49 (1997).
82. E. Thomas, in *Late Paleocene Early Eocene Climatic and Biotic Events in the Marine and Terrestrial Records*, M. P. Aubry, S. G. Lucas, W. A. Berggren, Eds. (Columbia Univ. Press, New York, 1998), pp. 214–243.
83. G. Y. Lu, T. Adatte, G. Keller, N. Ortiz, *Eclogae Geol. Helv.* **91**, 293 (1998).
84. E. M. Crouch *et al.*, *Geology* **29**, 315 (2001).
85. P. L. Koch, J. C. Zachos, D. L. Dettman, *Palaeogeogr. Palaeoclimatol. Palaeoecol.* **115**, 61 (1995).
86. W. C. Clyde, P. D. Gingerich, *Geology* **26**, 1011 (1998).
87. S. L. Wing, in (*85*), pp. 380–400.
88. K. C. Beard, M. R. Dawson, *Bull. Soc. Geol. Fr.* **170**, 697 (1999).
89. S. Bains, R. D. Norris, R. M. Corfield, K. L. Faul, *Nature* **407**, 171 (2000).
90. D. J. Beerling, *Palaeogeogr. Palaeoclimatol. Palaeoecol.* **161**, 395 (2000).
91. J. G. Baldauf, in *Eocene-Oligocene Climatic and Biotic Evolution*, D. A. Prothero, W. A. Berggren, Eds. (Princeton Univ. Press, Princeton, NJ, 1992), pp. 310–326.
92. E. Thomas, J. C. Zachos, T. J. Bralower, in *Warm Climates in Earth History*, B. Huber, K. G. MacLeod, S. L. Wing, Eds. (Cambridge Univ. Press, New York, 2000), pp. 132–160.
93. The calcite compensation depth (CCD) represents the depth in the ocean at which dissolved carbonate ion content [CO_3] transitions from being saturated to undersaturated. Virtually no biogenic calcite is preserved in sediments beneath this level, which at present is roughly 4500 m in the Atlantic and 3500 m in the Pacific. Because the degree of [CO_3] saturation is sensitive to fluxes of respired CO_2 and dissolved ions to the ocean, the CCD is constantly changing with time.
94. T. H. Van Andel, *Earth Planet. Sci. Lett.* **26**, 187 (1975).
95. N. J. Shackleton, M. A. Hall, I. Raffi, L. Tauxe, J. Zachos, *Geology* **28**, 447 (2000).
96. D. R. Prothero, W. A. Berggren, Eds., *Late Eocene-Oligocene Climatic and Biotic Evolution* (Princeton Univ. Press, Princeton, NJ, 1992).
97. R. E. Fordyce, *Am. Paleontologist* **8**, 2 (2000).
98. J. A. Wolfe, in *Cenozoic Climate and Paleogeographic Changes in the Pacific Region*, K. Ogasawara, J. A. Wolfe, Eds. (1994).
99. E. N. Edinger, M. J. Risk, *Palaios* **9**, 576 (1994).
100. M. Pagani, M. A. Arthur, K. H. Freeman, *Paleoceanography* **14**, 273 (1999).
101. P. Huybrechts, *Geografiska Annaler Stockholm* **75A**, 221 (1993).
102. L. R. Bartek, S. A. Henrys, J. B. Anderson, P. J. Barrett, *Mar. Geol.* **130**, 79 (1996).
103. N. W. Driscoll, G. H. Haug, *Science* **282**, 436 (1998).
104. L. J. Lourens, F. J. Hilgen, *Quat. Int.* **40**, 43 (1997).
105. B. Cramer, *Earth Planet. Sci. Lett.*, in press.
106. W. F. Ruddiman, A. McIntyre, *Science* **212**, 617 (1981).
107. N. G. Pisias, A. C. Mix, R. Zahn, *Paleoceanography* **5**, 147 (1990).
108. T. J. Crowley, K.-Y. Kim, J. G. Mengel, D. A. Short, *Science* **255**, 705 (1992).
109. T. D. Herbert, *Proc. Natl. Acad. Sci. U.S.A.* **94**, 8362 (1997).
110. G. R. Dickens, M. M. Castillo, J. C. G. Walker, *Geology* **25**, 259 (1997).
111. G. R. Dickens, *Bull. Soc. Geol. Fr.* **171**, 37 (2000).
112. J. C. Zachos, G. R. Dickens, *GFF* **122**, 188 (2000).
113. K. Kaiho *et al.*, *Paleoceanography* **11**, 447 (1996).
114. T. J. Bralower *et al.*, *Geology* **25**, 963 (1997).
115. M. E. Katz, D. K. Pak, G. R. Dickens, K. G. Miller, *Science* **286**, 1531 (1999).
116. S. P. Hesselbo *et al.*, *Nature* **406**, 392 (2000).
117. A. Berger, M. F. Loutre, *Quat. Sci. Rev.* **10**, 297 (1991).
118. N. J. Shackleton, M. A. Hall, A. Boersma, *Initial Reports of the Deep Sea Drilling Project* (U.S. Government Printing Office, Washington, DC, 1984), vol. 74, pp. 599–612.
119. P. J. Barrett, C. J. Adams, W. C. McIntosh, C. C. Swisher, G. S. Wilson, *Nature* **359**, 816 (1992).
120. S. W. Wise, J. R. Breza, D. M. Harwood, W. Wei, in *Controversies in Modern Geology* (Academic, San Diego, CA, 1991), pp. 133–171.
121. W. U. Ehrmann, A. Mackensen, *Palaeogeogr. Palaeoclimatol. Palaeoecol.* **93**, 85 (1992).
122. J. C. Zachos, J. R. Breza, S. W. Wise, *Geology* **20**, 569 (1992).
123. W. Ehrmann, *Palaeogeogr. Palaeoclimatol. Palaeoecol.* **139**, 213 (1998).
124. P. F. Barker, P. J. Barrett, A. K. Cooper, P. Huybrechts, *Palaeogeogr. Palaeoclimatol. Palaeoecol.* **150**, 247 (1999).

125. Supported by NSF grant EAR-9814883.